

4.1 Introduction

The advent of bulk metallic glasses (BMG) has opened lot of scope of wide range of applications for this class of amorphous materials. BMG's can be synthesized with relatively lower cooling rate with ease now. However, the glass formation in these systems seems to depend on quite a few parameters like enthalpy of melting, reduced glass transition temperature, under cooling etc. A metallic alloy can be transformed into glassy state provided that the melt can be undercooled to sufficiently low temperature and occurrence of crystallization is avoided. If cooling rate is high enough then less time will be available for molecules to arrange themselves and crystallization will not occur, hence glass formation will be favored. Thermodynamics plays a very important role in glass formation in multi-component metallic alloys. Scientific efforts have made to predict glass forming ability (GFA) of metallic alloys, thermodynamically as well as kinetically, so that metallic glasses with excellent GFA can be designed [4.1-4.3]. Thermodynamically, Gibbs free energy difference is a good indicator of GFA [4.4]. The glass forming ability of metallic alloy can be expressed in terms of critical cooling rate (R_c) or critical size (Z_c). The parameter that describes GFA is the cooling rate R_c , needed to prevent formation of detectable amount of crystals upon quenching the materials from liquid state and Z_c is the maximum size of material up to which it can remain in fully amorphous state. Between R_c and Z_c , R_c is more suitable to represent GFA as Z_c is dependent on fabrication method rather than alloy composition [4.5]. Bulk glass forming alloys are distinguished from each other by their critical cooling rates for vitrification. So R_c is a ideal route to

determine the GFA of metallic alloy. R_c is a direct and universal measurement of the GFA of any substance including the conventional oxide glasses. Therefore, a complete understanding of GFA should be supported by an accurate and precise calculation of R_c .

The quantitative measure of the GFA is R_c above which no crystallization occurs when melt is solidified. Also, lower R_c always corresponds to higher GFA [4.6]. The critical cooling rate (R_c) depends on three factors: nucleation rate and its temperature variation, crystal growth rate and its temperature dependence and relationship between the two quantities and volume fraction (X) [4.7]. While a large number of empirical factors have been proposed over the past decades and correlated the GFA of various metallic glasses with R_c .

The experimental measurement of R_c involves series of continuous cooling experiments. To evaluate GFA by R_c for different alloy systems number of solidification trials with different cooling rates are necessary. A number of methods have been devised to determine R_c [4.8]. The most common method is to construct time-temperature-transformation (TTT) curve for the evaluation of R_c based on homogenous nucleation mechanism developed by Uhlmann [4.5]. TTT curve, describes the transformation kinetics from undercooled liquid to crystal in an isothermal experiment. From a practical standpoint, the TTT curves provide the temperature-time window for processing of bulk glass forming alloys without undesirable crystallization effects. The calculation of R_c basically involves three factors [4.9] 1.computational model to calculate critical volume fraction

crystallized 2.expression to calculate nucleation and growth rate 3.evaluation of several parameters used in nucleation and growth equations. From the knowledge of above criteria, theoretically R_c can be determined by TTT curves.

During solidification crystallization occurs which is a two step process i.e. nucleation and growth. Hence TTT curves give the transformation of nucleation controlled to growth controlled crystallization [4.9]. This method is also known as ‘Nose method’ [4.7].

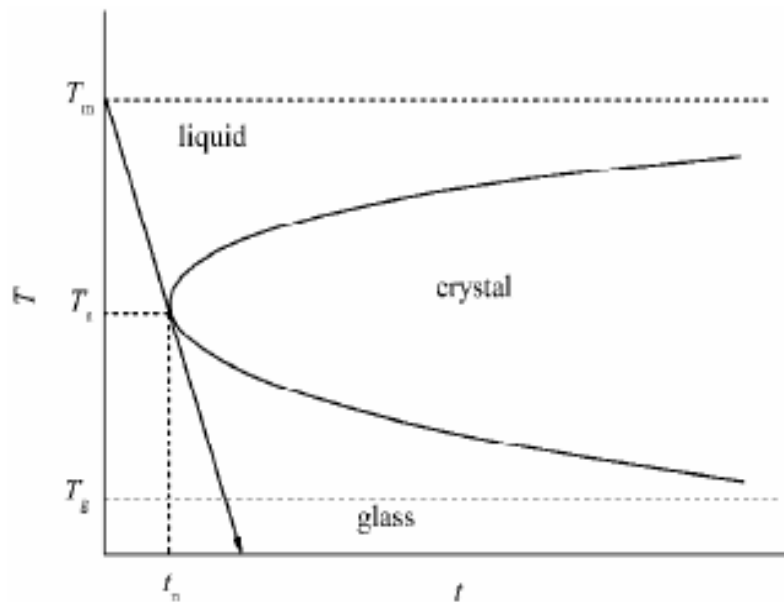


Fig. 4.1 Schematic TTT diagram

For the formation of metallic glass it is necessary to cool the liquid quickly enough to bypass the nose on the TTT diagram for crystallization. In general, the curves in TTT diagrams exhibit a “C-type” form with respect to time and temperature on x-axis and y-axis respectively, as shown schematically in fig. 4.1 and T_m , T_n and t_n represents the melting temperature, nose temperature and nose

time respectively. The nose of the TTT diagram corresponds to the temperature and time at which the material crystallizes the fastest. Thus, the nose defines through its temperature T_n and time t_n , the minimum cooling rate for which phase transformation occurs [4.10]. If the cooling rate is fast enough to avoid crystallization at the nose the material will form a glass. The shape and position of the TTT curve in the temperature-time space is determined by the intrinsic nucleation and growth mechanism. Therefore, TTT curves provide insight into the crystallization behavior of bulk metallic glasses. However, nucleation and growth of crystals influences kinetics of glass that may change the position and shape of the TTT curve [4.11-4.12].

BMGs have a lower thermodynamic driving force towards crystal nucleation and growth than ordinary metallic glasses, resulting in the nose of the TTT diagram being pushed out to longer times. With lower value of R_c and thicker sections of material can be cast amorphous alloys, if the nose of the TTT diagram is pushed out to longer times. Therefore, BMGs have an increased glass forming ability due to their increased liquid stability [4.13-4.14]. For glassy alloys the nose of the TTT curve is shifted to the right, thus providing more time to undergo phase transition. This TTT kinetic approach allows the minimal cooling rate and the general temperature time dependence for the phase transformation from the amorphous or glassy state to the crystalline state. It is observed that the nose method of predicting R_c is in reasonably good agreement with other methods [4.15].

4.2 Theoretical formulation

4.2.1 Expressions for Nucleation and growth

The volume fraction of crystallized material in an undercooled liquid alloy is very small so the critical volume fraction X can be expressed as [4.5,4.16]:

$$X = \frac{\pi}{3} I_v u^3 t^4 \quad (4.1)$$

where I_v is the steady state nucleation rate, u is the crystal growth rate and t is the time taken for X to crystallize.

The I_v can be written as [4.17]

$$I_v = \frac{A}{\eta(T)} \exp\left(-\frac{\Delta G^*}{k_B T}\right) \quad (4.2)$$

where A is the fitting parameter given by the following equation:

$$A \approx \frac{N_A}{V_m} \frac{k_B T}{3\pi a_0^3} \quad (4.3)$$

with a_0 being the average atomic diameter

and
$$\Delta G^*(T) = 16\pi\sigma^3 / 3[\Delta G(T)/V_m]^2 \quad (4.4)$$

where ΔG is the Gibbs free energy difference between liquid and crystalline phases, η is the temperature dependent viscosity of molten alloy, k_B is the Boltzman constant, V_m is the molar volume and $\sigma(T)$ is the temperature dependent interfacial energy using the enthalpy of fusion given as [4.18]:

$$\sigma(T) = \frac{\alpha\Delta H_m}{(N_A V_m^2)^{1/3}} \frac{T}{T_m} \quad (4.5)$$

where $\alpha=0.76$ for all Pd based metallic systems.

For constructing TTT curve, the temperature dependence of viscosity (η) of Pd based alloys is essential. The estimation of the viscosity for Pd based alloys is based on Vogel-Fulcher-Tamman (VFT) equation:

$$\eta(T) = \eta_0 \exp\left(\frac{DT_0}{T-T_0}\right) \quad (4.6)$$

where η_0 , D and T_0 are constants, which are necessary to be determined in order to obtain the expression of the viscosity.

The crystal growth u can be expressed by [4.19]:

$$u = f \frac{D}{a_0} \left[1 - \exp\left(-\frac{\Delta G}{RT}\right) \right] \quad (4.7)$$

where
$$D = \frac{k_B T}{3\pi a_0 \eta(T)} \quad (4.8)$$

with
$$f \approx 0.2(T_m - T)/T_m \quad (4.9)$$

So, to construct TTT diagram and to understand overall transformation kinetics of the amorphous alloys all parameters such as ΔG , σ , $\eta(T)$ need to be determined.

4.2.2 Estimation of Gibbs free energy difference

The Gibbs free energy difference (ΔG) plays an important role in for the prediction of R_c . ΔG , between undercooled melt and corresponding crystalline solid, acts as the driving force for crystallization. In an amorphous alloy system, lower value of ΔG indicates less driving force of crystallization, which enhances stability of metallic supercooled liquid and leads to better glass forming ability.

The expression for ΔG can be written as

$$\Delta G = \frac{\Delta H_m \Delta T}{T_m} - \int_T^{T_m} \Delta C_p dT + T \int_T^{T_m} \Delta C_p \frac{dT}{T} \quad (4.10)$$

If the experimental specific heat data is available for the undercooled and the crystal phases of a material, experimental ΔG values can be calculated with the help of above eq. (4.10). However in absence of experimental ΔG values one has to switch to suitable expression of ΔC_p that effectively represents the temperature dependence of ΔC_p . Several models [4.20-4.24] have been proposed for determination of ΔG with varying degrees of complexity which are available in literature. Most of these expressions of ΔG based on different variation of ΔC_p are discussed in chapter-3 in detail along with the merits and demerits of all expressions. All these analytical expressions consider some kind of assumption for the temperature dependence of the heat capacity.

Different assumption of ΔC_p works quite well for most of the glass forming systems and provides fairly close results for ΔG . But, for few systems having outstanding glass forming ability (GFA), temperature variation of ΔC_p has to be accounted for in some form. For bulk glass forming alloys having excellent GFA it is observed that the specific heat increases considerably with undercooling. Thus, Dhrunder et al [4.25] derived the expression of ΔG considering the hyperbolic variation of ΔC_p .

ΔC_p at any temperature in the undercooled region can be expressed as

$$\Delta C_p = \frac{\Delta C_p^m T_m}{T} \quad (4.11)$$

ΔC_p^m being the specific heat difference at the melting point. Substituting ΔC_p from Eq. (4.11) in Eqs.(4.10), the expression of ΔG can be written as follows;

$$\Delta G = \frac{\Delta H_m \Delta T}{T_m} - \Delta C_p^m T_m \left[\ln \frac{T_m}{T} - \frac{\Delta T}{T_m} \right] \quad (4.12)$$

Different expressions of ΔG , which are based on different ΔC_p variations, are used to calculate ΔG in the entire undercooled region for five different Pd based systems. The results obtained are compared with the experimental results and the GFA of different Pd based metallic glasses are discussed in the light of thermodynamic aspect.

These ΔG values by different expressions and experimental value of ΔG are incorporated in nucleation and growth equation to obtain TTT curves which finally determines R_c for different Pd based metallic glasses.

4.2.3 Estimation of Critical cooling rate (R_c) using TTT curves

A TTT diagram corresponding to a critical volume fraction of $X=10^{-6}$ can be constructed by substituting the expression of $\eta(T)$ and the different expressions of ΔG , the corresponding TTT curves for Pd based alloys can be obtained. So the R_c for the glass formation of Pd based alloys can be given by nose method [4.7] as:

$$R_c = \frac{T_m - T_n}{t_n} \quad (4.13)$$

where T_m is the melting temperature, T_n and t_n are the temperature and time

corresponding to the nose of TTT curves, respectively.

4.2.4 Expression for mixing enthalpy and entropy for multicomponent amorphous alloys.

Inoue [4.26] suggested three empirical rules for determining the GFA of metallic glass. One criterion of which is negative heat of mixing for glass formation. The mixing enthalpy of stable metallic liquid can be given by [4.27]:

$$\Delta H^{mix} = 4 \sum_{i=1, i \neq j}^n \Delta H_{AB}^{mix} C_i C_j \quad (4.14)$$

where, ΔH^{mix} is the mixing enthalpy between A and B components, C_i is the atomic percentage of i^{th} component..

The mixing entropy for multicomponent system can be given by following equation [4.28]:

$$\Delta S^{mix} = -R \sum_{i=1}^n C_i \ln \varphi_i \quad (4.15)$$

where R is the gas constant, φ_i is the atomic volume fraction of the i^{th} component and can be written as:

$$\varphi_i = \frac{C_i r_i^3}{\sum_{i=1}^n C_i r_i^3} \quad (4.16)$$

where r_i is the atomic radius.

4.3 Results and discussion

4.3.1 Determination of ΔG using different theoretical models for Pd based metallic systems.

Several Pd based alloys form BMGs which are known for their good GFA. Many studies have been reported to evaluate GFA for Pd based metallic glasses [4.29-4.30]. Nishiyama et al [4.31] reported that Pd₄₀Cu₃₀P₂₀Ni₁₀ have high GFA with low critical cooling of 0.1 K/s for glass formation and maximum size is about 72 mm by water quenching technique. Also Xu et al [4.32] demonstrated that the accurate experimental determination of some parameters, which are crucial for calculating R_c , is difficult. So they have drawn some random values of parameters and using the classical theory examined probabilistic distribution of R_c for Pd-based metallic glasses. Kim et al [4.33] evaluated R_c for different metallic glasses by combining continuous cooling transformation (CCT) and continuous heating transformation (CHT) curves. More recently Xu et al [4.34] have calculated R_c for Fe-based metallic alloy by Uhlmann [4.5] and Barandiaran-Colmenero method. In Uhlmann method different expressions of ΔG and different models of viscosity ($\eta(T)$) were examined and it was found that R_c obtained by Thompson-Speapen (TS) [4.21] expression for ΔG was in accordance with the experimental result. Ge et al [4.35] have used Davies Uhlmann kinetic formulation to construct TTT curves of Cu-Zr binary alloys and found that R_c obtained using TS equation for ΔG gives better results than Turnbull equation. In the present study, we have investigated the GFA of five different Pd based alloys by calculating ΔG values in entire undercooled region, using different expressions available in literature [4.20-4.25]. Various expressions used here are based on different dependence of ΔC_p on temperature.

A low value of ΔG implies that a larger embryo for nucleation is required, which will require greater chemical fluctuations. Hence the value of ΔG between liquid and crystal phases will be smaller [4.36]. Small ΔG also indicates small free volume in a metallic glass. This enhances the formation of short range order in the alloy near melting point. So, for a good glass forming system, the values of ΔG and R_c need to be smaller. A smaller value of ΔG indicates smaller nucleation (I_v) and growth rates (u), as indicated by expressions (4.2) & (4.7). Lower I_v and u corresponds to lower crystallization rate, hence greater GFA. In order to check the applicability of various GFA parameters, they are correlated with R_c . So, determination of R_c is important for studying the GFA of metallic glasses. The evaluation of R_c requires the knowledge of ΔG . $\Delta G (T_g)$ is a good indicator of the glass forming ability of metallic glasses. The $\Delta G (T_g)$ values for different alloy compositions, by different theoretical approaches, are shown in table 4.1.

Table 4.1 $\Delta G (T_g)$ values for various Pd-based alloys by different methods

Systems	$\Delta G(T_g)$ (kJ/mol)						
	Expt [4.30]	Dhurandhar et al (Hyperbolic)	Lad-1	Lad-2	Turnbull	Singh & Holz	TS
Pd ₄₀ Ni ₄₀ P ₂₀	2953.83	2954.84	2631.44	2240.10	3553.83	3308.48	2881.07
Pd ₄₀ Cu ₄₀ P ₂₀	2400.00	2288.41	2152.76	1816.68	3183.12	2913.66	2404.72
Pd _{77.5} Cu ₆ Si _{16.5}	2030.77	2110.51	1895.55	1603.43	2685.71	2695.87	2075.17
Pd ₄₆ Cu _{35.5} P _{18.5}	1497.44	1518.49	1642.46	1399.00	2211.09	2059.74	1758.78
Pd _{42.5} Cu ₃₀ Ni _{7.5} P ₂₀	1312.82	1315.75	1442.76	1254.44	1794.82	1699.57	1500.49

It can be observed from the table 4.1 that expression given by Dhurandhar et al provides value of $\Delta G (T_g)$ very close to the experimental values for all the Pd-based alloys. It can also be observed from table 4.1 that among various Pd-based alloys, Pd_{42.5}Cu₃₀Ni_{7.5}P₂₀ system possesses the lowest value of $\Delta G (T_g)$. Hence it

has the highest GFA. This is in accordance with the Inoue's empirical rules [4.26, 4.37], which states that the GFA of a metallic glass increases with the increase in the number of alloying elements. Even a minor change in composition of metallic glasses affects the GFA greatly. From above compositions, it can be seen that minor addition of Ni to Pd₄₀Cu₄₀P₂₀ alloy increases its GFA by almost twice the value.

The variation in $\Delta G(T_g)$ values by different expression for Pd based metallic glasses may be due to a reason that all the expressions of ΔG are derived using different approximation of ΔC_p . Turnbull expression considers ΔC_p to be equal to zero. In general, ΔC_p is found to decrease with increase in temperature for metallic glasses. Also ΔG does not increase rapidly and shows saturation at large ΔT . Since, Turnbull expression does not involve any variation in ΔC_p with temperature; hence it provides good results in smaller undercooled region, but fails to account for non-linearity in large undercooled region for metallic glasses. Further, the expressions given by Lad et al [4.23-4.24] are based on constant ΔC_p approximation, given by $\Delta C_p = \Delta H_m / T_m$. These expressions fairly explain the non linearity in ΔG , particularly at large ΔT , for few metallic glass systems and it clearly shows the improvement of the proposed Lad et al expressions over Turnbull expression [4.20]. Also these expressions are widely used for metallic glasses, since they require lesser number of experimental parameters for ΔG calculations. But they fail to explain the variation of ΔG with temperature for a wide range of metallic glasses.

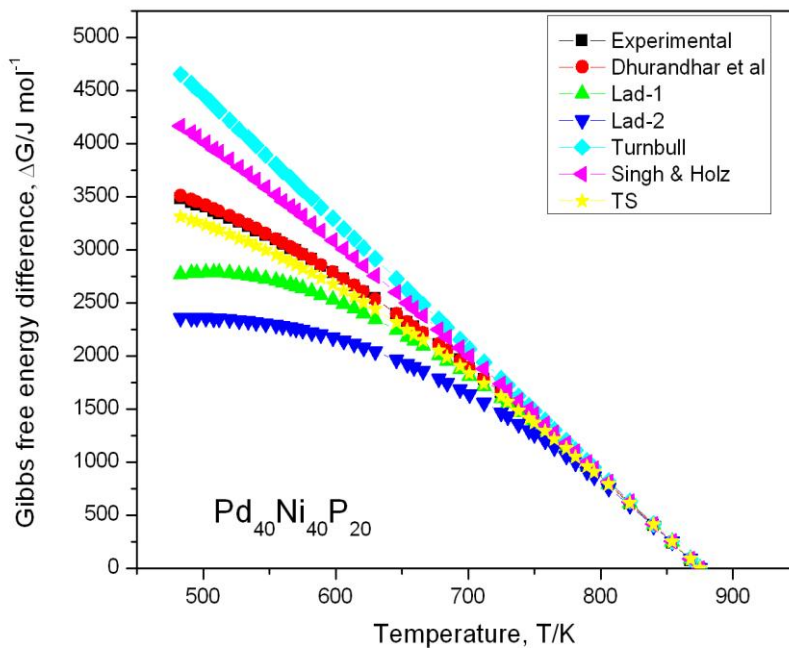


Fig 4.2 Variation of ΔG with temperature for $\text{Pd}_{40}\text{Ni}_{40}\text{P}_{20}$ metallic glass

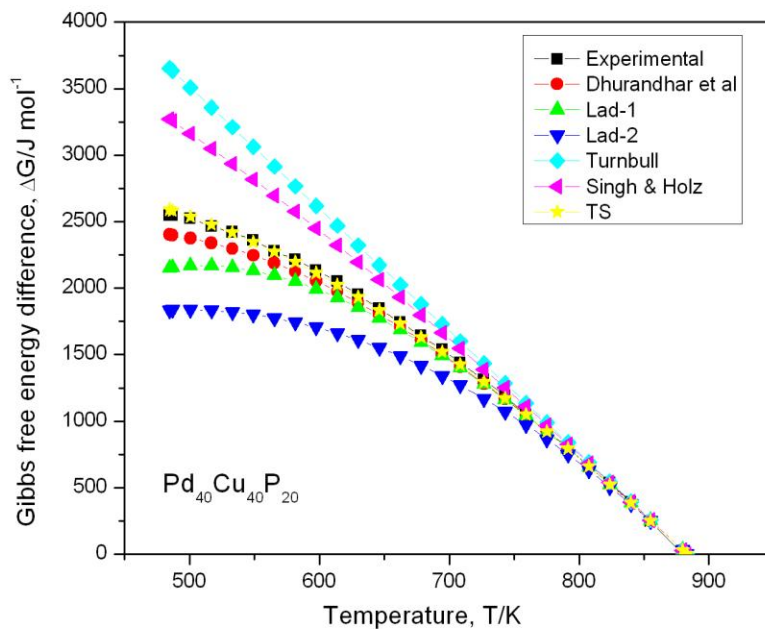


Fig. 4.3 Variation of ΔG with temperature for $\text{Pd}_{40}\text{Cu}_{40}\text{P}_{20}$ metallic glass

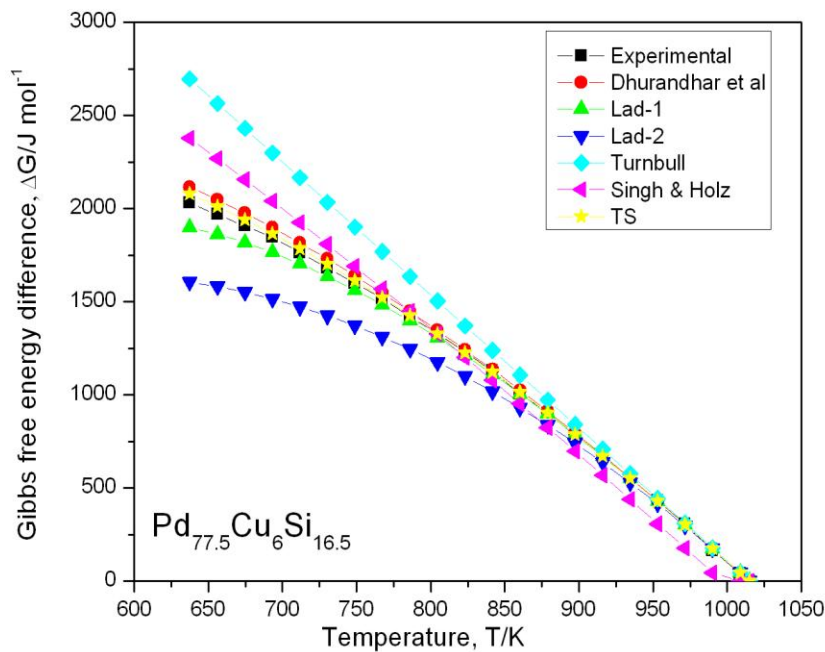


Fig. 4.4 Variation of ΔG with temperature for $\text{Pd}_{77.5}\text{Cu}_6\text{Si}_{16.5}$ metallic glass

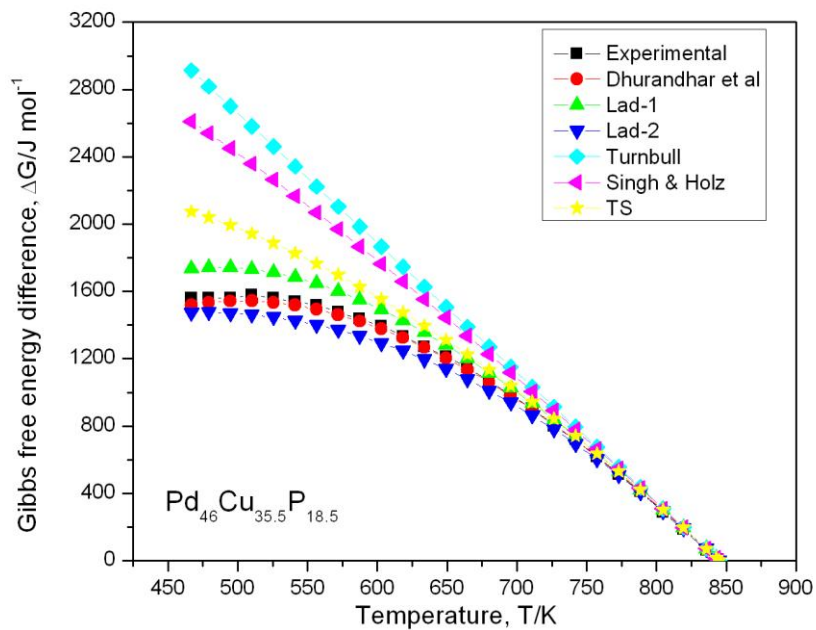


Fig.4.5 Variation of ΔG with temperature for $\text{Pd}_{46}\text{Cu}_{35.5}\text{P}_{18.5}$ metallic glass

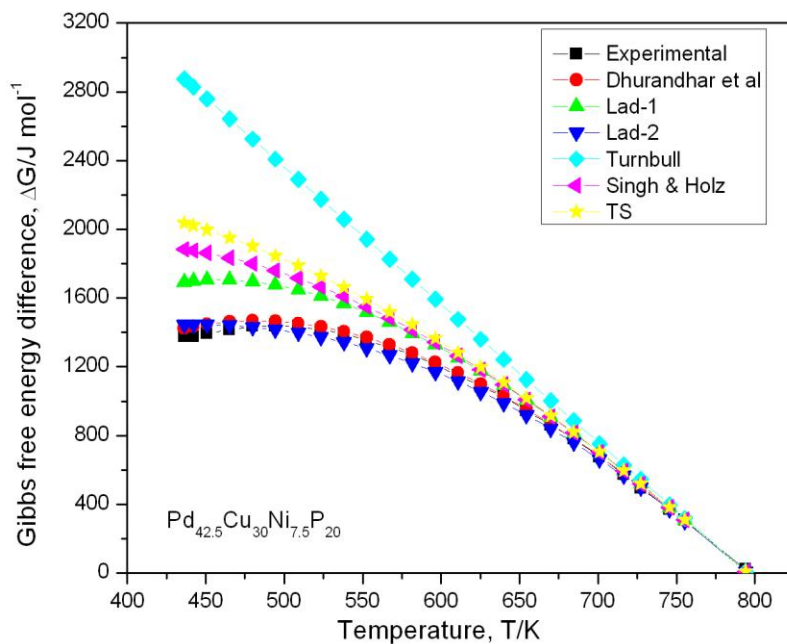


Fig.4.6 Variation of ΔG with temperature for $\text{Pd}_{42.5}\text{Cu}_{30}\text{Ni}_{7.5}\text{P}_{20}$ metallic glass

Figures 4.2-4.6 show variation of ΔG with temperature, calculated by different theoretical approaches. It can be observed from fig.4.2-4.4 that for alloys $\text{Pd}_{40}\text{Cu}_{40}\text{P}_{20}$, $\text{Pd}_{40}\text{Ni}_{40}\text{P}_{20}$, and $\text{Pd}_{77.5}\text{Cu}_6\text{Si}_{16.5}$, the expressions given by Lad et al underestimate the experimental values in the entire undercooled region. Hence, Lad-1 and Lad-2 expressions show different variation for different glassy systems and therefore they are not suitable to study the variation of ΔG for Pd-based metallic glasses. It can be seen from fig. 4.3 and fig. 4.4 that for $\text{Pd}_{40}\text{Cu}_{40}\text{P}_{20}$ and $\text{Pd}_{77.5}\text{Cu}_6\text{Si}_{16.5}$ metallic glasses, the values of ΔG obtained by TS expression superimposes the experimental values. But for other three systems it does not give accurate results. It can be observed from fig. 4.6 that for $\text{Pd}_{42.5}\text{Cu}_{30}\text{Ni}_{7.5}\text{P}_{20}$ metallic glass, the result obtained by Lad-2 expression lies in close agreement

with the experimental values of ΔG , but Lad-1 overestimates the experimental values. ΔG values were also calculated using expression given by Dhurandhar et al [4.25]. The values obtained by this expression perfectly matches with the experimental values in all systems. ΔG values calculated by this expression also provide a good match with the experimental results in the entire undercooled region as observed from fig. 4.2-4.6.

Furthermore, we have also used expression given by Singh & Holz [4.22], which involves linear variation of ΔC_p with temperature. Moreover, it is derived using an ansatz for explaining the temperature dependence of ΔC_p . The values of ΔG calculated by this expression overestimate the experimental values for all Pd-based alloys. Hence it does not account for the variation of ΔG with T in entire undercooled region. TS expression explains the non linearity in the entire undercooled region. Turnbull expression for ΔG was used which gives very crude results in case of BMGs.

4.3.2 Glass forming ability of different Pd based metallic glasses

The GFA of metallic glasses are supposed to increase as size mismatch among the constituent atoms increase. The atomic radii of Pd, Ni, Cu, Si and P are 140pm, 149pm, 145pm, 110pm, 98pm respectively. It can be observed from the atomic size that for some glasses size mismatch does not effectively reflects the GFA of metallic glass, such as the GFA of Pd₄₀Ni₄₀P₂₀ metallic glass is smaller than that of Pd₄₀Cu₄₀P₂₀ metallic glass, although the atomic sizes of their components are almost same. So size mismatch cannot always justify the GFA of metallic glasses.

Another criterion for glass formation is negative heat of mixing. The mixing enthalpies and entropies of Pd-based metallic glasses are represented in table 4.2.

Table 4.2 Calculated mixing enthalpies and entropies, and critical sizes (Z_c) of Pd-based metallic glasses

Composition	$\Delta H^{mix}/\text{kJ mol}^{-1}$	$\Delta S^{mix}/\text{J K}^{-1}\text{mol}^{-1}$	Z_c/nm [4.30]
Pd ₄₀ Ni ₄₀ P ₂₀	-22.72	9.56	25
Pd ₄₀ Cu ₄₀ P ₂₀	-26.24	9.48	2
Pd _{77.5} Cu ₆ Si _{16.5}	-31.48	5.79	1
Pd ₄₆ Cu _{35.5} P _{18.5}	-26.15	9.14	12
Pd _{42.5} Cu ₃₀ Ni _{7.5} P ₂₀	-25.46	10.97	72

The mixing enthalpy (ΔH^{mix}) characterizes the chemical interactions between the constituent elements of the metallic glass. If the chemical interactions among the constituent elements of the glass are more, then the long distance diffusion of atoms becomes difficult [4.38]. Formation of local atomic clusters takes place that results in large negative mixing enthalpy and thereby large GFA. But if ΔH^{mix} values are very large, i.e., the components have a very strong interactions among themselves, it may result in the formation of stable crystal nuclei. Hence, a very large value of ΔH^{mix} may degrade the GFA of metallic glasses. On the other hand, if the chemical interactions are very small, long distance diffusion of atoms will occur easily and formation of new nuclei will take place thereby resulting in formation of new crystal structure. Thus, for the formation of a homogeneous glassy phase with a high GFA, the value of ΔH^{mix} should be moderate. Further, small mixing entropy implies less disordered atomic structures. The diffusion of

atoms becomes easier if the metallic glass is less disordered. Consequently, it takes less time for the liquid to form a new ordered structure. Hence the GFA of metallic glass becomes less. Therefore for good GFA high value of ΔS^{mix} is necessary. In present case, Pd_{77.5}Cu₆Si_{16.5} has the highest value of ΔH^{mix} and the lowest value of ΔS^{mix} , but it is neither the best nor the worst glass former among all the compositions. Pd_{42.5}Cu₃₀Ni_{7.5}P₂₀ is found to be the best glass former having moderate value of ΔH^{mix} and highest value of ΔS^{mix} . But, all the other glasses do not strictly follow the above mentioned criteria.

4.3.3 Effect of different model of ΔG in calculation of R_c for Pd based systems

Slower cooling rates impose a higher barrier for crystallization. In order to crystallize, the glass forming melt requires a large amount of energy to overcome the energy barrier. Hence, crystallization becomes difficult at slower cooling rates, which thereby increases the ability of the metallic alloy to form glass. The knowledge of R_c provides an insight it to study the GFA of metallic glasses. Weinberg et al [4.39] explained that R_c is sensitive to material parameters which are present in I_v and u expressions. Since the evaluation of I_v and u requires many parameters to be determined, theoretical approximations for various parameters are considered.

Xu et al [4.40] fitted the experimental TTT curves for Pd₄₀Cu₃₀P₂₀Ni₁₀ and Zr_{41.2}Ti_{13.8}Cu_{12.5}Ni₁₀Be_{22.5} metallic glasses, by varying different parameters in nucleation and growth expression. Then R_c was calculated by continuous integral

method in the framework of classical theory. In present work, various expressions of ΔG discussed above are used to calculate I_v and u for Pd-based alloys. Finally TTT curves are constructed using Davis Uhlmann's theory [4.5] for homogeneous nucleation in the framework of classical nucleation theory.

Table 4.3 Critical cooling rate (R_c) values for various Pd-based alloys by different methods

Alloys	Critical cooling rate R_c /(Ksec ⁻¹)		
	Expt [4.30]	Dhurandhar et al	Lad-1
Pd ₄₀ Ni ₄₀ P ₂₀	3.83x10 ⁻⁶	2.1x10 ⁻⁶	4.9x10 ⁻⁸
Pd ₄₀ Cu ₄₀ P ₂₀	7.60x10 ⁻³	1.23x10 ⁻³	5.01x10 ⁻⁴
Pd _{77.5} Cu ₆ Si _{16.5}	1.30	0.9	0.161
Pd ₄₆ Cu _{35.5} P _{18.5}	5.95x10 ⁻⁵	1.59x10 ⁻⁵	2.49x10 ⁻⁴
Pd _{42.5} Cu ₃₀ Ni _{7.5} P ₂₀	2.51x10 ⁻⁸	1.08x10 ⁻⁸	4.17x10 ⁻⁷

Table 4.3 Continued.....

Alloys	Critical cooling rate R_c /(Ksec ⁻¹)			
	Lad-2	Turnbull	Singh & Holz	TS
Pd ₄₀ Ni ₄₀ P ₂₀	4.09x10 ⁻¹¹	2.53x10 ⁻⁴	4.61x10 ⁻⁵	4.77x10 ⁻⁷
Pd ₄₀ Cu ₄₀ P ₂₀	1.93x10 ⁻⁶	0.346	0.1	2.88x10 ⁻³
Pd _{77.5} Cu ₆ Si _{16.5}	1.61x10 ⁻³	35.01	11.33	0.60
Pd ₄₆ Cu _{35.5} P _{18.5}	1.63x10 ⁻⁶	0.088	0.026	1.01x10 ⁻³
Pd _{42.5} Cu ₃₀ Ni _{7.5} P ₂₀	1.38x10 ⁻⁹	6.70x10 ⁻⁵	6.70x10 ⁻⁵	1.65x10 ⁻⁶

The R_c values, determined from TTT curves using different expressions of ΔG , are shown in table 4.3. It indicates that R_c obtained using different expression of ΔG

vary within few orders of magnitude than the experimental result. The R_c values obtained by Turnbull and Singh & Holz method overestimates the value of R_c calculated by using experimental ΔG , whereas Lad-1 & Lad-2 underestimate the results. The variation in the value of R_c by different model of ΔG may be due to reason that all the expression are derived from different approximation of ΔC_p . However the result obtained by Dhurandhar et al expression clearly indicate that it gives better agreement with experimental data in calculating R_c for glass transition of Pd-based alloys. Therefore, this should be appropriate for determining ΔG for Pd-based alloys. So, the variation in ΔG affects the calculation of R_c due to the change in location of maximum crystallization rate.

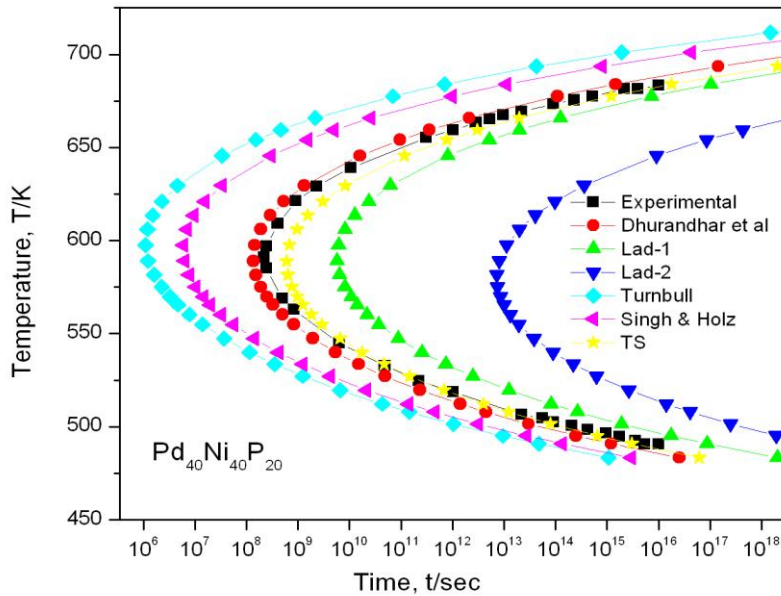


Fig. 4.7 Calculated TTT curves for Pd₄₀Ni₄₀P₂₀ metallic glass by different expressions of ΔG

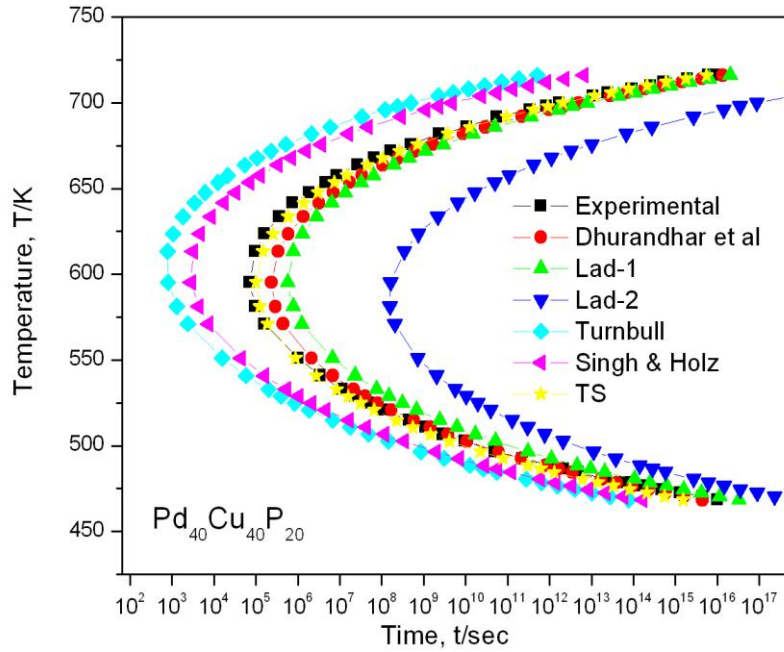


Fig. 4.8 Calculated TTT curves for $\text{Pd}_{40}\text{Cu}_{40}\text{P}_{20}$ metallic glass by different expressions of ΔG

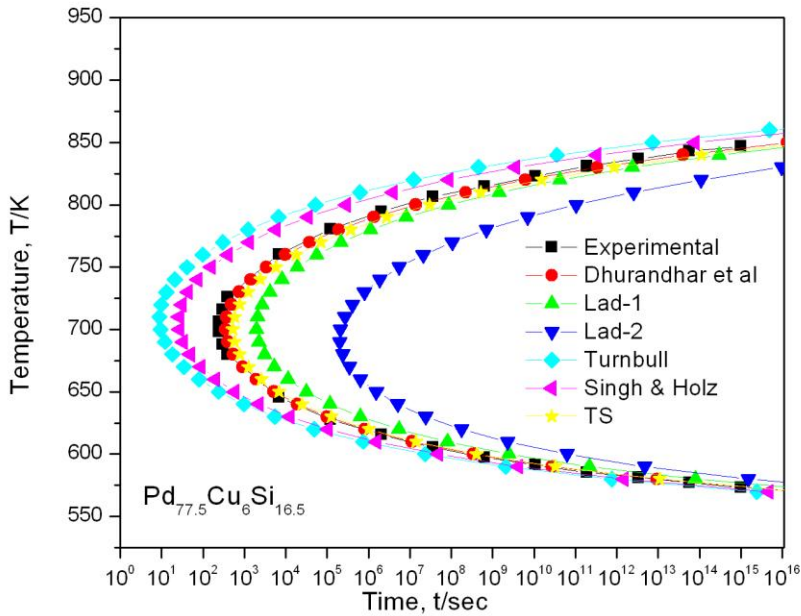


Fig. 4.9 Calculated TTT curves for $\text{Pd}_{77.5}\text{Cu}_6\text{Si}_{16.5}$ metallic glass by different expressions of ΔG

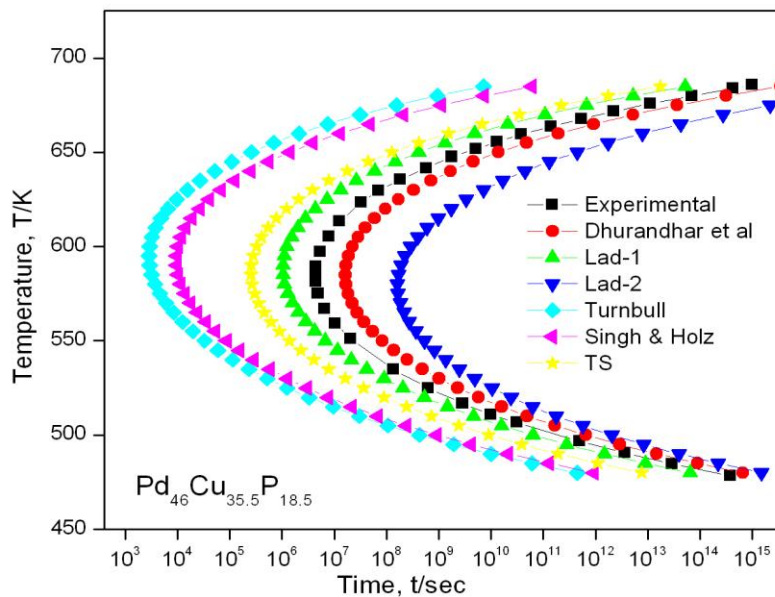


Fig. 4.10 Calculated TTT curves for $\text{Pd}_{46}\text{Cu}_{35.5}\text{P}_{18.5}$ metallic glass by different expressions of ΔG

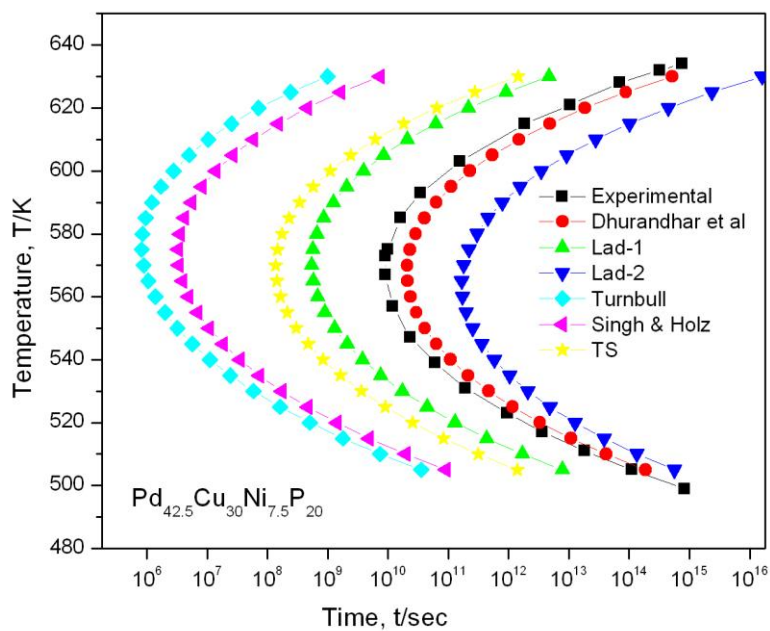


Fig. 4.11 Calculated TTT curves for $\text{Pd}_{42.5}\text{Cu}_{30}\text{Ni}_{7.5}\text{P}_{20}$ metallic glass by different expressions of ΔG .

The value of R_c obtained suggests that calculated results reflect the GFA of Pd-based alloys. The TTT curves of the Pd-based alloy calculated by application of different models of ΔG are shown in figures 4.7-4.11. The TTT curves results in “C” shape because of competition between increasing driving force for crystallization and slowing down of kinetics (effective diffusivity) of atom movement [4.41]. Also during the non isothermal cooling the major contribution for the total volume crystallized comes from the temperature region in the vicinity of nose [4.7]. The transformation (liquid-to-crystal) accelerates with an increase in under-cooling. The maximum transformation rate is obtained at the nose of the TTT curve. It can be seen that at the nose point cooling rate is high enough to form a glass. Below nose temperature the driving force for transformation continues to increase but the reaction is now impeded by slow diffusion. Hence, the position of nose in the TTT curve determines the R_c to be used in order to obtain glass. By application of different theoretical expressions of ΔG in nucleation and growth rate equation, it can be observed that the nose of TTT curve is shifted significantly. The decrease in driving force results in decrease in R_c due to shifting of nose towards longer time, which reflects better GFA. So, the calculation of R_c depends on the temperature range under consideration. In small undercooled region the theoretical ΔG values lies close to experimental values, so if R_c is calculated in this region, the choice of expression for ΔG will not make any significant difference in results.

It is observed from fig 4.7-4.11, that when the number of components increases from 3 to 4, the C-curve shifts towards right, i.e., the metallic alloy can stay in its

super-cooled liquid state for a longer time thereby reducing its R_c and increasing GFA. In present case, t_n for $\text{Pd}_{46}\text{Cu}_{35.5}\text{P}_{18.5}$ metallic glass is of the order 10^6 sec, whereas for $\text{Pd}_{42.5}\text{Cu}_{30}\text{Ni}_{7.5}\text{P}_{20}$ it is of the order 10^9 sec. So, an increase in number of components reduces R_c and increases GFA.

Based on high Z_c and low R_c values, the alloys can be arranged in increasing order of GFA as $\text{Pd}_{40}\text{Ni}_{40}\text{P}_{20}$, $\text{Pd}_{40}\text{Cu}_{40}\text{P}_{20}$, $\text{Pd}_{77.5}\text{Cu}_6\text{Si}_{16.5}$, $\text{Pd}_{46}\text{Cu}_{35.5}\text{P}_{18.5}$ and $\text{Pd}_{42.5}\text{Cu}_{30}\text{Ni}_{7.5}\text{P}_{20}$. It can be seen from table 4.2, that $\text{Pd}_{42.5}\text{Cu}_{30}\text{Ni}_{7.5}\text{P}_{20}$ alloy has highest value of Z_c and lowest value of R_c and ΔG . This proves its better GFA over all other metallic glasses. On the other hand, $\text{Pd}_{40}\text{Ni}_{40}\text{P}_{20}$ metallic glass is supposed to have second highest GFA, next to the $\text{Pd}_{42.5}\text{Cu}_{30}\text{Ni}_{7.5}\text{P}_{20}$ alloy, based on its second highest Z_c value and smaller R_c value. But ΔG values are not able to reflect the same order of GFA for these metallic glasses.

4.3.4 Estimation of Critical Cooling Rate for Binary Metallic Glasses using TTT Diagram

4.3.4.1 Gibbs free energy difference and TTT curves for binary metallic glasses

In the present work, the binary system Cu-Zr is studied as it has excellent GFA. Xu et al [4.42] studied $\text{Cu}_{100-x}\text{Zr}_x$ alloy in the composition range $x=34$ to 40 at.% and reported that $\text{Cu}_{64}\text{Zr}_{36}$ is the best GFA composition and $\text{Cu}_{46}\text{Zr}_{54}$ has critical thickness for glass formation up to 2mm which is highest of its compositional range[4.43]. Tang et al. [4.44] studied GFA in the $\text{Cu}_{100-x}\text{Zr}_x$ system for $x=40$ to 55 at.% and concluded that $\text{Cu}_{50}\text{Zr}_{50}$ rods could be cast completely amorphous

with diameter up to 2mm. In the present paper critical cooling rate and the critical diameter for the $\text{Cu}_{54}\text{Zr}_{46}$ and $\text{Cu}_{50}\text{Zr}_{50}$ are calculated. The TTT curves and critical cooling rates are estimated by using Davies-Uhlmann formulation.

In the present study, we investigated the GFA of two Cu-Zr alloys. The molar free energy i.e. driving force for crystallization (G_m) is calculated using Lad et al expressions [4.23-4.24]. The variation of G_m between under-cooled liquid and corresponding crystalline solid with temperature is shown graphically in fig. 4.12 & fig. 4.13 respectively for $\text{Cu}_{54}\text{Zr}_{46}$ and $\text{Cu}_{50}\text{Zr}_{50}$.

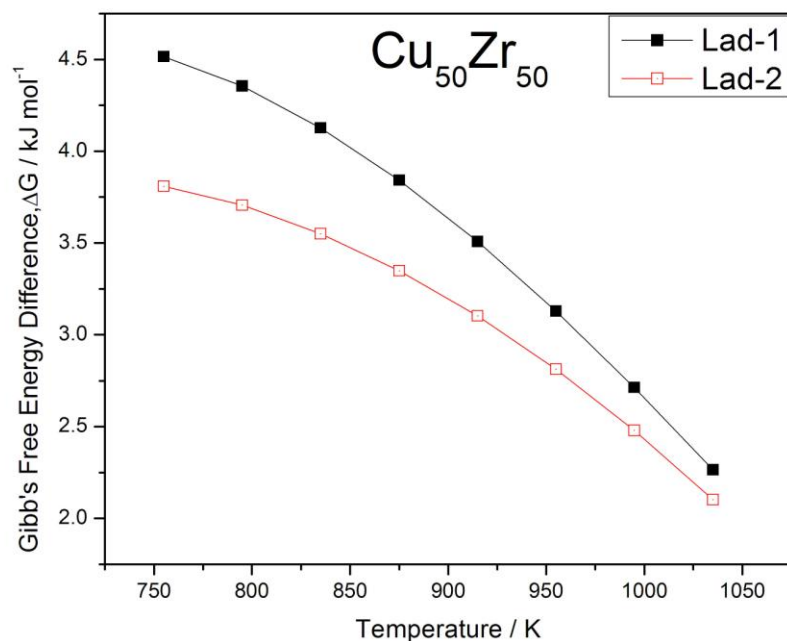


Fig. 4.12 Variation of Gibbs free energy difference with temperature for $\text{Cu}_{50}\text{Zr}_{50}$

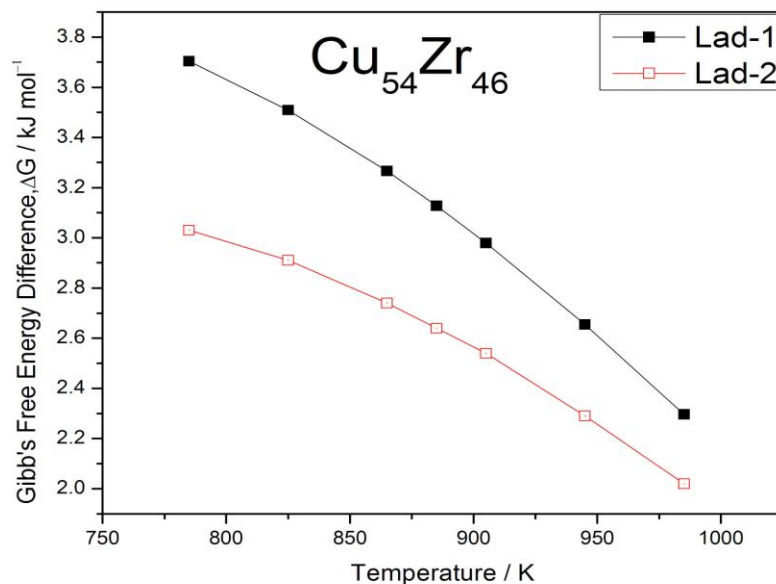


Fig.4.13 Variation of Gibbs free energy difference with temperature for $\text{Cu}_{54}\text{Zr}_{46}$

The dependence of driving force on under-cooling temperature is different for Lad-1 and Lad-2 methods. Hence their effect on critical cooling rate will be different for both the systems. It is obvious from the G_m values obtained for this system that it has fairly good glass forming ability owing to smaller value of G_m . By calculating the time required for forming a crystallization volume of X based on growth kinetics, the TTT curves can be obtained and a nose appears as a result of a competition between the driving force for crystallization, which increases with decreasing temperature, and atomic mobility, which decreases with decreasing temperature. In constructing these TTT curves, the time required to transform the volume fraction at a given temperature is calculated using Uhlmann formulation for a particular fraction crystallized and these calculation is repeated for other temperatures.

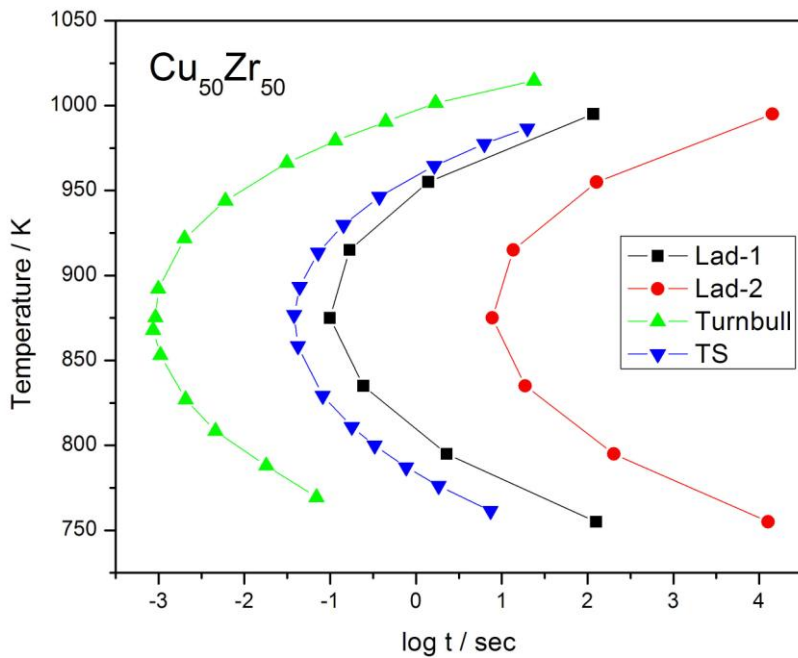


Fig. 4.14 TTT curves for $\text{Cu}_{50}\text{Zr}_{50}$

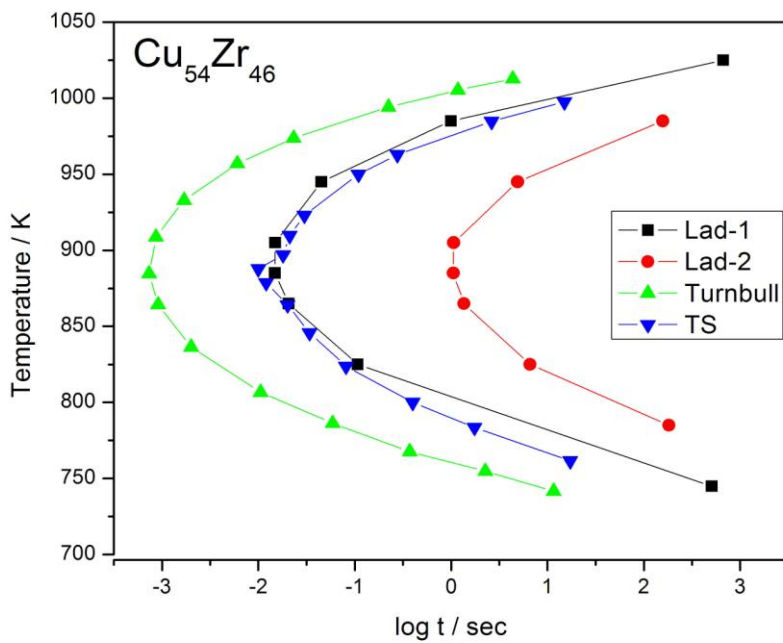


Fig. 4.15 TTT curves for $\text{Cu}_{54}\text{Zr}_{46}$

In TTT diagram the time to transform volume fraction is plotted as a function of temperature. The TTT curves of the Cu-Zr alloys are calculated by application of different expressions for G_m . Here TTT curves are obtained for two different systems i.e. $\text{Cu}_{54}\text{Zr}_{46}$ and $\text{Cu}_{50}\text{Zr}_{50}$ as shown in fig. (4.14) & fig. (4.15) respectively.

From the figures 4.14 & 4.15 it can be observed that a nose shape graph appears which indicates the time scale to reach onset of crystallization. The nose in a TTT curve corresponds to the least time for the volume fraction to crystallize. The TTT curves for $\text{Cu}_{54}\text{Zr}_{46}$ and $\text{Cu}_{50}\text{Zr}_{50}$ by Lad-1 shows good agreement with those obtained by Thomson Spaepen.

4.3.4.2 Estimation of Critical size from R_c for binary alloys

Lin and Johnson [4.45] noted that the maximum diameters (d_{max}) for which samples are fully amorphous can be used to estimate critical cooling rate (R_c) according to following equation:

$$R_c (K / s) = \frac{10}{\{d(cm)\}^2}$$

For both the alloy compositions, critical cooling rate (R_c) and critical diameter (d_{max}) calculated by different methods are shown in table 4.4.

Table 4.4 Critical cooling rate R_c and d_{max} for different Cu-Zr metallic systems

Sr. No	Different methods	Alloy compositions			
		Cu ₅₄ Zr ₄₆		Cu ₅₀ Zr ₅₀	
		R_c (K/s)	d_{max} (mm)	R_c (K/s)	d_{max} (mm)
1	Lad-1	2.1×10^4	0.21	3.3×10^3	0.55
2	Lad-2	2.9×10^2	1.84	42.97	4.82
3	Turnbull	2.8×10^5 [4.35]	0.05	3.8×10^5	0.05
4	Thompson Spaepen (TS)	1.2×10^4 [4.35]	0.28	9.9×10^3	0.31

It is observed from table that the critical cooling rate is smallest obtained from Lad-2 method. The critical cooling rates evaluated by Lad-1 method are in good agreement with TS for Cu₅₄Zr₄₆ and Cu₅₀Zr₅₀. The calculated critical cooling rates of Cu₅₀Zr₅₀ by Lad-1 & Lad-2 are lower than Cu₅₄Zr₄₆. It is observed that the critical cooling rates calculated by Lad-2 are lower than calculated by other methods and vary within few orders of magnitude. This indicates that the molar free energy driving force for crystallization plays an important role in predicting the critical cooling rates.

The critical cooling rates of Cu₅₀Zr₅₀ are calculated to be 42.97 K.s⁻¹ and 3.3×10^3 K.s⁻¹ by Lad-2 & Lad-1 respectively. But the experimental data for Cu₅₀Zr₅₀ is found to be 250 K.s⁻¹ [4.46] which is much lower than other reported result except for Lad-2 method. The calculated R_c for Cu₅₀Zr₅₀ by lad-2 is lower than the experimental result.

Hence the maximum diameter for which $\text{Cu}_{54}\text{Zr}_{46}$ and $\text{Cu}_{50}\text{Zr}_{50}$ remains amorphous are calculated. The results indicate that critical diameter for both the alloys are smaller than 1mm except for d obtained by Lad-2. For $\text{Cu}_{50}\text{Zr}_{50}$ rods it is also reported that if a diameter $d \leq 2\text{mm}$ then it is fully amorphous and if $d \geq 3\text{mm}$ they are partially crystalline[4.46]. Hence it can also be concluded that for $\text{Cu}_{50}\text{Zr}_{50}$ if $d=2\text{mm}$ then R_c will be 250 K.s^{-1} . So $\text{Cu}_{50}\text{Zr}_{50}$ rods with good GFA can be formed.

4.4 Conclusions

The thermodynamic behaviour of BMGs have been studied by estimating ΔG for five samples of Pd-based metallic glasses using expressions obtained by different approximation of ΔC_p and the results obtained are very close to the experimental values. It can also be concluded that larger ΔS^{mix} and moderate ΔH^{mix} is necessary for the metallic alloys for a high GFA. Also calculated data indicate that the better the GFA of Pd-based metallic glasses, the lesser the value of ΔG between supercooled liquid and the crystalline phase. The R_c values for the glass formation of Pd-based metallic glasses have been estimated by TTT calculations. Computation of the TTT curves was based on Uhlmann's assumptions [4.5]. Different models of ΔG were incorporated in nucleation and growth rate expression to evaluate R_c . The result obtained by expression given by Dhurandhar et al (hyperbolic) for ΔG gives the best estimation for R_c for the glass formation of Pd based alloys. The driving force of crystallization affects the estimation of R_c in large undercooled region, but in lower undercooling it does not make a significant

difference. The present study suggests that the thermodynamic quantity ΔG of the under cooled liquid is indispensable for estimation of TTT curves. Pd_{42.5}Cu₃₀Ni_{7.5}P₂₀ metallic glass is found to be the best glass former among all Pd-based metallic glasses.

The critical cooling rates for Cu₅₄Zr₄₆ and Cu₅₀Zr₅₀ were estimated using Uhlmann's method. In Uhlmann's method, the driving force for crystallization from the under-cooled liquid for Cu-Zr binary alloys is determined using Lad-1 & Lad-2 expressions. The values of R_c calculated by Lad-1 method is found to be lower than that calculated by Lad-2 method by the order of two magnitudes for both the alloy compositions. On comparing the result of TTT curves, the critical cooling rates obtained by Lad-1 are found to be in good agreement with TS. Regarding the critical size, d , from table-1 it is evident that for Cu₅₀Zr₅₀ Lad-1 estimates value of d (=0.55mm) close to the experimental value, i.e., 2mm. Hence, it can be concluded that TTT curves gives better estimation of critical cooling rates. So this can be treated as a good method for predicting glass forming ability and to obtain the critical size for fully amorphous structure. Also, it can be concluded that Cu₅₀Zr₅₀ is a better glass former than Cu₅₄Zr₄₆.

References

- [4.1] P.K Singh, K.S Dubey. *J Therm Anal Calorim.* **100**; (2010):347.
- [4.2] J. Wu, Y. Pan, J. Huang, J. Pi. *Thermochim Acta.* **552**; (2013):15.
- [4.3] J.E.K Schawe. *J Therm Anal Calorim.* **120**; (2015):1417.
- [4.4] A.T Patel, H.R Shevde, A. Pratap. *J Therm Anal Calorim.* **107**; (2012):167.
- [4.5] D.R Uhlmann. *J.Non-cryst.Solids* **7**; (1972):337.
- [4.6] A. Inoue. *Acta Mater.* **48**; (2000):279.
- [4.7] M.C Weinberg, D.R Uhlmann. *J.Am.Ceram.Soc.* **72**; (1989):2054-8
- [4.8] S. Guo, Z.P Lu, C.T. Liu. *Intermetallics.* **18**; (2010):883.
- [4.9] J. Schroers, Y. Wu, R. Busch, W.L Johnson. *Acta mater.***49**; (2001):2773.
- [4.10] I. Gutzow , I. Avramov , K. Kästner , *J. Non-Cryst. Solids* **123**; **1990**:97 .
- [4.11] T. D. Shen and R. B. Schwarz. *Appl. Phys. Lett.* **75**; (1999):49.
- [4.12] J. Schroers, Y. Wu, and W. L. Johnson. *Phil. Mag.* **82**; (2002):1207.
- [4.13] W. H. Wang, C. Dong, and C. H. Shek. *Mat. Sci. and Eng. R* **44**; (2004) 46.
- [4.14] R. Busch, *JOM* **52**; (2000):39.
- [4.15] D.R Uhlmann, L. Klein, P.I.K Onorato, R.W Hopper. *Proc.Lunar Sci. Conf. 6th* (1975):693.
- [4.16] N. Nishiyama, A. Inoue. *Acta Mater* **47**(5); (1999):1487.
- [4.17] D. Herlach. *Mater. Sci. Eng. R* **12**; (1994):177.
- [4.18] W.A Miller, G.A Chadwick. *Acta. Metall.* **15**(4); (1967):607.

- [4.19] C. Kittel. *Introduction to Solid State Physics* (John Wiley & Sons, New York, 2005):71
- [4.20] D. Turnbull, *J. Appl. Phys.* **21**; (1950):1022.
- [4.21] C.V. Thompson and F. Spaepen, *Acta Metall.*, **27**; (1979):1855.
- [4.22] H.B. Singh and A. Holz, *Solid State Commun.*, **45**; (1983):985.
- [4.23] K.N. Lad, Arun Pratap and K.G. Raval, *J. Mater. Sci. Lett.* **21**; (2002):1419
- [4.24] K.N. Lad, K.G. Raval and Arun Pratap, *J. Non-Cryst. Solids* **334 & 335**; (2004):259.
- [4.25] H. Dhurandhar, T.L.S Rao, K.N Lad, A. Pratap. *Philos. Mag. Lett.* **88(4)**; (2008):239.
- [4.26] A. Inoue, A. Takeuchi, T. Zhang. *Metall. Mater. Trans*, **29A**; (1998):1779.
- [4.27] M. Xia, S. Zhang, J. Li, C. Ma. *Appl Phys Lett.* **88**; (2006):261913.
- [4.28] Q. Jiang, B.Q Chi, J.C Li. *Appl Phys Lett.* **82**; (2003):2984.
- [4.29] N. Nishiyama, A. Inoue. *Mater.Trans.* **43(8)**; 2002:1913.
- [4.30] O. Haruyama, T. Watanabe, K. Yuki, M. Horiuchi, H. Kato, N. Nishiyama. *Physical Review B* **83**; (2011):064201.
- [4.31] N. Nishiyama, A. Inoue. *Mater. Trans. JIM* **38(5)**; (1997):464.
- [4.32] D. Xu, B.D Wirth, J. Schroers, W.L Johnson. *App.Phys.Lett.* **97**; (2010):024102.
- [4.33] J.H Kim, J.S Park, E.S Park, W.T Kim, D.H Kim. *Metals and Materials Int.* **11(1)**; (2005):1.
- [4.34] K. Xu, Y. Wang, J. Li, Q. Li. *Acta Metallurgica Sinica* **26(1)**; 2013:56.

- [4.35] Li Ge, X. Hui, G. Chen, Z. Liu. *Acta Phys.Chim.Sin* **23(6)**; (2007):895.
- [4.36] F. Guo, S. Poon, G. Shiflet. *Appl.Phys.Lett.* **83(13)**; (2003):2575.
- [4.37] A. Inoue. *Mater Trans JIM.* **36**; (1995):866.
- [4.38] D. Wang, Y. Huang, J. Shen. *J Non-Cryst Solids.* **355**; (2009):986.
- [4.39] M.C Weinberg, B.J Zelinski, D.R Uhlmann. *J. Non-Cryst. Solids* **123**;
(1990):90.
- [4.40] D. Xu, W.L Johnson. *Phys.Rev.B* **74**; (2006):024207.
- [4.41] D.R Uhlmann. *J. Non-Cryst. Solids* **25**; (1977):42.
- [4.42] D. Xu, B. Lohwongwatana, G. Duan, W.L Johnson, C. Garland. *Acta
Mater.***52**; (2004):2621.
- [4.43] D. Xu, G. Duan, W.L Johnson. *Phys Rev Lett.* **92**; (2004):245504.
- [4.44] M.B Tang, D.Q Zhao, M.X Pan, W.H Wang. *Chin Phys Lett.* **21**; (2004):
901.
- [4.45] X.H Lin, W.L Johnson. *J Appl Phys.* **78**; (1995):6514.
- [4.46] W.H Wang, J.J Lewandowski, A.L Greer. *J Mater Res.* **20(9)**; (2005):
2307.